System Size, Energy, and Centrality Dependence of Pseudorapidity Distributions of Charged Particles in Relativistic Heavy-Ion Collisions

B. Alver,[1] B. B. Back,[1] M. D. Baker,[2] M. Ballintijn,[4] D. S. Barton,[2] R. R. Betts,[6] R. Bindel,[7] W. Busza,[4] Z. Chai,[2] V. Chetluru,[6] E. García,[6] T. Gburek,[3] K. Gulbrandsen,[4] J. Hamblen,[8] I. Harnarine,[6] C. Henderson,[4] D. J. Hofman,[6] R. S. Hollis,[6] R. Hołyński,[3] B. Holzman,[2] A. Iordanova,[6] J. L. Kane,[4] P. Kulinich,[4] C. M. Kuo,[5] W. Li,[4] W. T. Lin,[5] C. Loizides,[4] S. Manly,[8] A. C. Mignerey,[7] R. Nouicer,[2] A. Olszewski,[3] R. Pak,[2] C. Reed,[4] E. Richardson,[7] C. Roland,[4] G. Roland,[4] J. Sagerer,[6] I. Sedykh,[2] C. E. Smith,[6] M. A. Stankiewicz,[2] P. Steinberg,[2] G. S. F. Stephans,[4] A. Sukhanov,[2] A. Szostak,[2] M. B. Tonjes,[7] A. Trzupek,[3] G. J. van Nieuwenhuizen,[4] S. S. Vaurynovich,[4] R. Verdier,[4] G. I. Veres,[4] P. Walters,[8] E. Wenger,[4] D. Willhelm,[7] F. L. H. Wolfs,[8] B. Wosiek,[3] K. Woźniak,[3] S. Wyngaardt,[2] and B. Wysłouch[4]

(PHOBOS Collaboration)

[1]*Argonne National Laboratory, Argonne, Illinois 60439-4843, USA*
[2]*Brookhaven National Laboratory, Upton, New York 11973-5000, USA*
[3]*Institute of Nuclear Physics PAN, Kraków, Poland*
[4]*Massachusetts Institute of Technology, Cambridge, Massachusetts 02139-4307, USA*
[5]*National Central University, Chung-Li, Taiwan*
[6]*University of Illinois at Chicago, Chicago, Illinois 60607-7059, USA*
[7]*University of Maryland, College Park, Maryland 20742, USA*
[8]*University of Rochester, Rochester, New York 14627, USA*

(Received 27 September 2007; revised manuscript received 4 August 2008; published 6 April 2009)

We present the first measurements of the pseudorapidity distribution of primary charged particles in Cu + Cu collisions as a function of collision centrality and energy, $\sqrt{s_{NN}} = 22.4$, 62.4, and 200 GeV, over a wide range of pseudorapidity, using the PHOBOS detector. A comparison of Cu + Cu and Au + Au results shows that the total number of produced charged particles and the rough shape (height and width) of the pseudorapidity distributions are determined by the number of nucleon participants. More detailed studies reveal that a more precise matching of the shape of the Cu + Cu and Au + Au pseudorapidity distributions over the full range of pseudorapidity occurs for the same $N_{\text{part}}/2A$ rather than the same N_{part}. In other words, it is the collision geometry rather than just the number of nucleon participants that drives the detailed shape of the pseudorapidity distribution and its centrality dependence at RHIC energies.

DOI: 10.1103/PhysRevLett.102.142301 PACS numbers: 25.75.Dw

The advent of Cu + Cu collisions from the Relativistic Heavy-Ion Collider (RHIC) at energies similar to those of the earlier Au + Au collisions presents a new opportunity to measure the system size dependence of important observables such as the pseudorapidity density of charged particles, $dN_{\text{ch}}/d\eta$, using different collision geometries. The observed $dN_{\text{ch}}/d\eta$ is an experimentally well-defined quantity which is sensitive to the initial conditions of the system, i.e., parton shadowing, and also to the effects of rescattering and hadronic final-state interactions. The Cu + Cu results are expected to provide critical tests of the parametric dependence of $dN_{\text{ch}}/d\eta$ and a constraint on the mechanism underlying charged particle production. Also they serve as a bridge between Au + Au [1–3] and d + Au [4,5] results in terms of the number of participant nucleons, N_{part}, as well as allowing for a direct comparison to Au + Au results at the same N_{part}.

In this Letter, we present the first measurements of the $dN_{\text{ch}}/d\eta$ of primary charged particles over a broad range of pseudorapidity, $|\eta| < 5.4$, for Cu + Cu collisions at a variety of collision centralities at three energies, $\sqrt{s_{NN}} =$ 22.4, 62.4, and 200 GeV. The present Cu + Cu results are compared to our previous results from Au + Au [2,3] and d + Au [4,5] collisions. We would like to stress that the Cu + Cu, Au + Au, and d + Au data at all energies were obtained using the same detector setup in the PHOBOS experiment. This is optimal because common systematic errors cancel in the ratio. This led us to perform a comprehensive examination of particle production in Cu + Cu and Au + Au collisions for the same number of nucleon participant pairs, for the same fraction of total inelastic cross section and for the same geometry in both systems. Additionally, the Cu + Cu, Au + Au, and d + Au results allow us to study the interplay between collision energy and system size.

The data were obtained with the multiplicity array [6]. The array consists of an octagonal barrel of silicon detectors, the octagon, covering $|\eta| \leq 3.2$. This array is augmented by two sets of three annular silicon counter arrays, the rings, covering $3.0 < |\eta| < 5.4$. Monte Carlo (MC)

TABLE I. The estimated number of nucleon participants, $\langle N_{\rm part}\rangle$, and the total charged particle multiplicity, $N_{\rm ch}^{\rm tot}$ for Cu + Cu collisions in different centrality bins are presented. All errors are systematic (90% C.L.).

	200 GeV		62.4 GeV		22.4 GeV	
Centrality (%)	$\langle N_{\rm part}\rangle$	$N_{\rm ch}^{\rm tot}$	$\langle N_{\rm part}\rangle$	$N_{\rm ch}^{\rm tot}$	$\langle N_{\rm part}\rangle$	$N_{\rm ch}^{\rm tot}$
0–3	106 ± 3	1541 ± 70	102 ± 3	833 ± 36	103 ± 3	535 ± 23
3–6	100 ± 3	1407 ± 68	95 ± 3	781 ± 34	95 ± 3	482 ± 21
6–10	91 ± 3	1262 ± 59	88 ± 3	721 ± 32	86 ± 3	431 ± 19
10–15	79 ± 3	1084 ± 51	76 ± 3	635 ± 27	74 ± 3	375 ± 18
15–20	67 ± 3	917 ± 43	65 ± 3	541 ± 24	63 ± 3	320 ± 15
20–25	57 ± 3	771 ± 38	55 ± 3	460 ± 21	53 ± 3	273 ± 14
25–30	47 ± 3	645 ± 32	47 ± 3	386 ± 17	44 ± 3	230 ± 13
30–35	40 ± 3	538 ± 27	38 ± 3	323 ± 15	37 ± 3	194 ± 12
35–40	33 ± 3	444 ± 23	32 ± 3	270 ± 13	30 ± 3	162 ± 12
40–45	27 ± 3	364 ± 19	25 ± 3	223 ± 11	25 ± 3	135 ± 11
45–50	22 ± 3	293 ± 15	21 ± 3	183 ± 9	20 ± 3	112 ± 11
50–55	17 ± 3	234 ± 13	16 ± 3	147 ± 8	16 ± 3	92 ± 11

simulations of the detector performance were based on the HIJING event generator [7] and GEANT [8] simulations, folding in the signal response for scintillator counters (paddles, covering $3.0 < |\eta| < 4.5$), and silicon sensors. In the present work, the Au + Au data at 19.6 GeV have been reanalyzed using an improved treatment of dead detector channels, resulting in a slightly smaller multiplicity (the largest difference is on the order of 5% at midrapidity in the most central bin) than given in previous publications [2,3]. However, the new results agree with the older results within the published systematic errors. The 19.6 GeV Au + Au data and the new Cu + Cu data were analyzed in the same way as the previously published data of Au + Au at 200 and 62.4 GeV [2,3], using two analysis methods [9], ''hit-counting'' and ''analog.'' The measured $dN_{\rm ch}/d\eta$ was corrected for particles which were absorbed or produced in the surrounding material and for feed-down products from weak decays of neutral strange particles. Uncertainties in $dN_{\rm ch}/d\eta$ associated with these corrections range from 6% in the octagon up to 28% in the rings for Cu + Cu, Au + Au, and d + Au measurements. These are the uncertainties common to all collision systems and they dominate the systematic errors. In the present work, the analog results were corrected for the overcounting of multiply charged fragments such as helium ions emitted in the forward regions. The correction, which was largest for the lowest energies and most peripheral collisions, changed the total number of charged particles by less than 6%, and has been taken into account in the systematic error assignments.

The centrality determination procedure applied for Cu + Cu collisions is the same as for Au + Au collisions at similar energies [2,3]. For the 200 and 62.4 GeV data sets, the centrality was estimated from the data using the truncated mean of the paddles signals. Using HIJING [7] and AMPT [10] models, we have estimated our minimum-bias trigger efficiency for events with a vertex near (±10 cm) the nominal interaction point to be 84 ± 5% and 75 ± 5% in Cu + Cu collisions at 200 and 62.4 GeV, respectively. At the lowest energies, 22.4 GeV (Cu + Cu) and 19.6 GeV (Au + Au), the much lower beam rapidity precludes the use of the paddles for centrality determination. Instead, we construct a different quantity, ''EOCT,'' the path-length-corrected sum of the energy deposited in the octagon. This procedure has been discussed in Ref. [2]. We use a Glauber

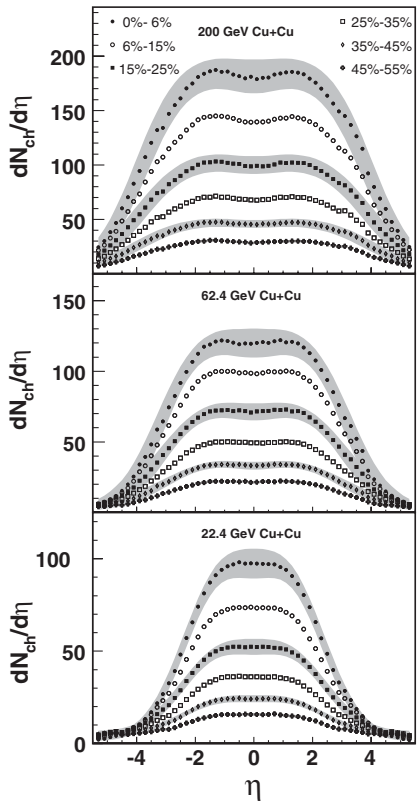

FIG. 1. $dN_{\rm ch}/d\eta$ distributions of primary charged particles from Cu + Cu collisions at $\sqrt{s_{NN}} = 22.4$, 62.4, and 200 GeV for the specified centrality bins. The typical systematic errors (90% C.L.) are shown as bands for selected centrality bins.

model calculation implemented in HIJING simulations to estimate $\langle N_{\rm part}\rangle$ for each centrality bin. The $\langle N_{\rm part}\rangle$ values for various centrality bins for Cu + Cu collisions are given in Table I.

Figure 1 shows the primary charged particle $dN_{\rm ch}/d\eta$ distributions measured in Cu + Cu collisions at $\sqrt{s_{NN}} =$ 22.4, 62.4, and 200 GeV for different centrality bins. The statistical errors are negligible. Both the height and width of the $dN_{\rm ch}/d\eta$ distributions increase as a function of energy as has been seen for Au + Au collisions [2].

The comparison of $dN_{\rm ch}/d\eta$ distributions for Cu + Cu and Au + Au collisions at similar energy is shown in Fig. 2. The distributions are normalized to $\langle N_{\rm part}\rangle$ and the goal is to study the sensitivity of the shape of the pseudorapidity distribution to the volume of the overlap region ($N_{\rm part}$), fraction of total inelastic cross section (centrality) or geometry ($N_{\rm part}/2A$). The geometry ($N_{\rm part}/2A$) is defined as the fraction of total nuclear volume which interacts. For centrality bins chosen so that the average number of participants in both systems is similar, Figs. 2(a)–2(c), the comparison shows that at 200 GeV the $dN_{\rm ch}/d\eta$ distributions in both systems agree within systematic errors, both in height and width, and that at 62.4 and 22.4 GeV, the distributions agree within systematic errors at midrapidity but not in the fragmentation regions (i.e., high $|\eta|$). The $dN_{\rm ch}/d\eta$ distributions of Au + Au collisions at 19.6 and 62.4 GeV have been interpolated linearly in $\ln(\sqrt{s_{NN}})$ to obtain the scaled Au + Au data at 22.4 GeV. We observe that the charged particle production in the high $|\eta|$ region is increased in Au + Au compared to Cu + Cu collisions. This increase of charged particles may be attributed to the two excited nuclear remnants being bigger in Au + Au

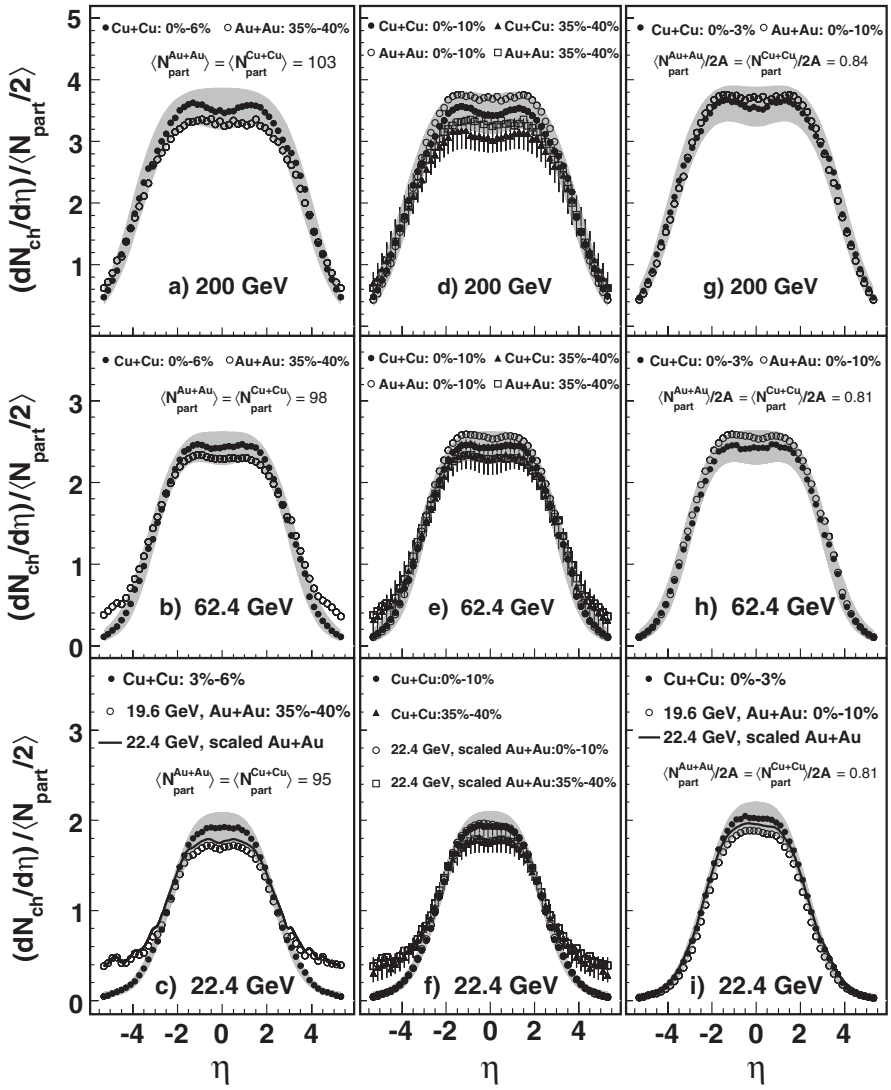

FIG. 2. $(dN_{\rm ch}/d\eta)/\langle N_{\rm part}/2\rangle$ distributions in Cu + Cu and Au + Au [2,3] collisions at 22.4 (19.6), 62.4, and 200 GeV selected to yield (a)–(c) similar $\langle N_{\rm part}\rangle$, (d)–(f) similar centrality bin (central 0%–10% and peripheral 35%–40%), (g)–(i) similar geometry, $\langle N_{\rm part}\rangle/2A$. The gray band and error bars indicate the systematic uncertainty (90% C.L.) for central and peripheral Cu + Cu collisions, respectively. Errors for Au + Au are not shown for clarity.

than in Cu + Cu collisions. This effect is most visible at the lowest energies where the broad η coverage gives access to $|\eta| > y_{\mathrm{beam}}$. For centrality bins chosen so that the fraction of total inelastic cross section (central 0%–10% and peripheral 35%–40%) in both systems is similar, Figs. 2(d)–2(f), the comparison shows, at the three energies, that the $dN_{\mathrm{ch}}/d\eta$ distributions in both systems agree within systematic errors over the full η coverage at a given centrality bin. A more detailed look indicates, however, that there is a difference between the distributions at high $|\eta|$. The effect is similar to the one observed in Figs. 2(a)–2(c) but at smaller magnitude. We conjecture that the effect is due to the different balance between the size of the participant and spectator parts of the nuclei (geometry). To check this we compare values of $N_{\mathrm{part}}/2A$ for both systems at different bins of the fraction of total inelastic cross section, as shown in Fig. 3(a), where A is the mass number of the colliding nuclei. We observe indeed that in bins more central than the bin of 15%–20% (fraction of total inelastic cross section >0.8) the geometry differs. Plotting $dN_{\mathrm{ch}}/d\eta$ distributions in centrality bins with similar values of $N_{\mathrm{part}}/2A$ (automatically have matching $N_{\mathrm{spec}}/N_{\mathrm{part}}$ values, where $N_{\mathrm{spec}} = 2A - N_{\mathrm{part}}$) in Au + Au and Cu + Cu systems confirms that we obtain a better matching over the full η coverage, see Figs. 2(g)–2(i), with results shown for central collisions. Similar comparisons for more peripheral bins lead to the same conclusion (not shown). The data of $dN_{\mathrm{ch}}/d\eta$ distributions for Cu + Cu and Au + Au collisions can be found in Ref. [11].

To further investigate the percentile cross section and $N_{\mathrm{part}}/2A$ scaling with more precision (smaller systematic errors), we examine the ratios of $dN_{\mathrm{ch}}/d\eta'/\langle N_{\mathrm{part}}/2\rangle$ for central and peripheral, denoted $R_{PC}^{N_{\mathrm{part}}}$, at different energies as a function of η' as shown in Figs. 3(b) and 3(c), where $\eta' \equiv \eta - y_{\mathrm{beam}}$ corresponds effectively to the rest frame of one of the colliding nuclei [2]. The advantage of the ratio, $R_{PC}^{N_{\mathrm{part}}}$, is that dominant common systematic uncertainties in the MC-based background correction cancel because they are largely detector based and independent of the system and centrality. The inset of Fig. 3(b) shows the previously published results for Au + Au collisions [3], indicating that the change in shape as a function of centrality is independent of beam energy. The ratios $R_{PC}^{N_{\mathrm{part}}}$ for Cu + Cu at three energies exhibit the same feature (solid points) in Fig. 3(b). By comparing to Au + Au results (open points) this ratio is found to be similar in the midrapidity region $-2.5 \leq \eta' \leq 1$, but in the region $\eta' > 1$ the ratio for Au + Au is higher. To study this difference, we plot in Fig. 3(c) the $R_{PC}^{N_{\mathrm{part}}}$ ratio for Cu + Cu and Au + Au for centrality bins selected to represent similar initial geometry (similar value of $N_{\mathrm{part}}/2A$) for the two systems. Using this comparison criterion we observe good agreement between the two systems over the full coverage.

The comparison presented in Figs. 2 and 3 reveals an interesting feature: the fact that $dN_{\mathrm{ch}}/d\eta/\langle N_{\mathrm{part}}/2\rangle$ distributions of central Cu + Cu and central Au + Au collisions are similar over the full detector coverage ($|\eta| < 5.4$) implies that charged particle production normalized to the number of nucleon participants is mostly driven by geometry, $N_{\mathrm{part}}/2A$.

The interplay between the system size and the collision energy is shown in Fig. 4. The scaled pseudorapidity particle densities, $(dN_{\mathrm{ch}}/d\eta')/\langle N_{\mathrm{part}}/2\rangle$ for Cu + Cu and Au + Au collisions for more central collisions, 0%–6% is shown in Fig. 4(a). The results suggest that in symmetric nucleus-nucleus collisions the particle density per nucleon participant pair at the midrapidity region does not depend on the size of the two colliding nuclei but only on the collision energy. In the fragmentation region, the phenomenon of extended longitudinal scaling observed in

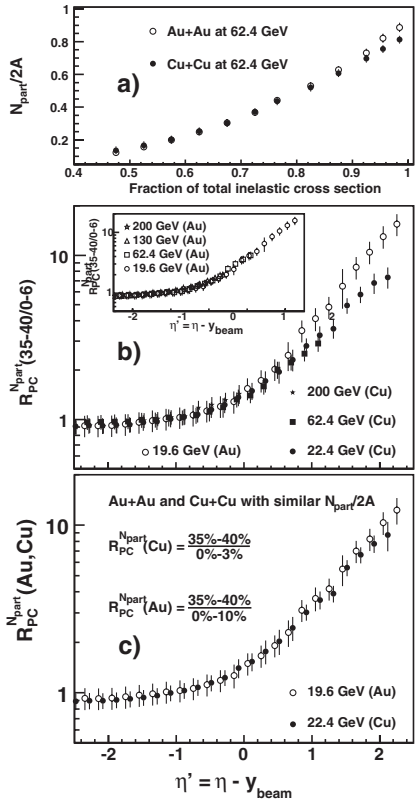

FIG. 3. (a) $\langle N_{\mathrm{part}}\rangle/2A$ versus fraction of the total inelastic cross section (centrality bin) for Cu + Cu and Au + Au collisions at 62.4 GeV (22.4 and 200 GeV give similar results). The ratio, $R_{PC}^{N_{\mathrm{part}}}(\eta')$, of $(dN_{\mathrm{ch}}/d\eta')/\langle N_{\mathrm{part}}/2\rangle$ (where $\eta' \equiv \eta - y_{\mathrm{beam}}$) for Cu + Cu and Au + Au collisions at RHIC energies is presented in (b) comparing the 35%–40% bin to the 0%–6% most central bin and (c) for centrality bins selected such that $N_{\mathrm{part}}/2A$ is similar for the two systems. The inset in (b) represents the ratio only for Au + Au data [3]. The error bars represent systematic errors (90% C.L.) on the ratio. Note that the scaled Au + Au at 22.4 GeV has not been added in the figure because the ratio, $R_{PC}^{N_{\mathrm{part}}}(\eta')$, for a given system is independent of energy. The values of $N_{\mathrm{part}}/2A$ for Cu + Cu and Au + Au are given in Fig. 2, and for 35%–40% collisions centrality at 22.4 (19.6) GeV are both equal to 0.24.

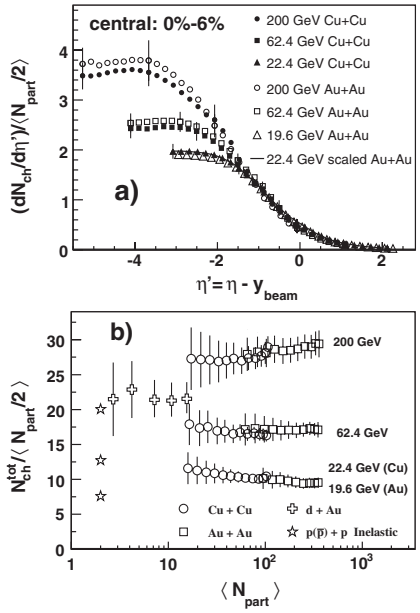

FIG. 4. (a) Cu + Cu and Au + Au [3] data, plotted as $(dN_{\rm ch}/d\eta')/\langle N_{\rm part}/2\rangle$ for 0%–6% most central events. (b) Integrated total of primary charged particle production obtained by extrapolating the data at each energy into the unmeasured region as a function of centrality in Cu + Cu collisions. The Au + Au, d + Au, and inelastic $p(\bar{p})$ + p data are taken from Refs. [3,5]. The uncertainty on $N_{\rm ch}^{\rm tot}$ and $N_{\rm part}$ has been included in the error bars.

Au + Au [1,2] and d + Au [5] collisions is also present in the Cu + Cu data. The Cu + Cu and Au + Au collisions exhibit the same extended longitudinal scaling in central collisions. This suggests that the extended longitudinal scaling holds independent of the collision energy and system size. The values of total charged particle multiplicity, $N_{\rm ch}^{\rm tot}$, estimated by extrapolation to the unmeasured region of pseudorapidity, are presented for Cu + Cu collisions at $\sqrt{s_{NN}} = 22.4$, 62.4, and 200 GeV in Fig. 4(b) and given in Table I. $N_{\rm ch}^{\rm tot}$ is obtained by averaging the results of two techniques, introduced in Ref. [12]. One involved fitting a Wood-Saxon functional form to the data for $|\eta| \leq 8$ at the two higher energies and $|\eta| \leq y_{\rm beam}$ at the lowest energy. The other involved simply integrating the lowest energy data and using the extended longitudinal scaling result to extrapolate the higher energy data into the unmeasured regions. The Cu + Cu and Au + Au results are compared at the same energies, 62.4 and 200 GeV, as well as at nearly the same energy 22.4 (Cu + Cu) and 19.6 GeV (Au + Au) in Fig. 4(b). We observe that $N_{\rm ch}^{\rm tot}$ scales approximately linearly with $\langle N_{\rm part}\rangle$ in both Cu + Cu and Au + Au collisions, and has similar values for the same $\langle N_{\rm part}\rangle$. The comparison indicates that the transition between inelastic $p(\bar{p})$ + p and Cu + Cu collisions is not controlled simply by the number of participants, as even the very central d + Au multiplicity per participant pair shows little sign of continuity to the Cu + Cu results, although we cannot exclude it, given the sizable systematic errors.

In summary, the results presented here show first measurements of pseudorapidity density distributions of primary charged particles and the estimated total charged particle multiplicity for Cu + Cu collisions as a function of collision centrality and energy, $\sqrt{s_{NN}} = 22.4$, 62.4, and 200 GeV. The Cu + Cu and Au + Au results at similar energy show that the particle density per nucleon participant pair in the midrapidity region is similar in both systems. The phenomenon of extended longitudinal scaling in Cu + Cu and Au + Au collisions holds independent of colliding energy and system size. The comparison of the results reveals an interesting feature that the best agreement of $(dN_{\rm ch}/d\eta)/\langle N_{\rm part}/2\rangle$ distributions over the full coverage, $|\eta| < 5.4$, for central and peripheral Cu + Cu and Au + Au collisions is obtained for centrality bins selected to yield similar geometry, i.e., similar value of $N_{\rm part}/2A$, in both systems. The essential role of collision geometry when comparing pseudorapidity distributions of charged particles across nuclear species is clearly demonstrated.

This work was partially supported by U.S. DOE grants No. DE-AC02-98CH10886, No. DE-FG02-93ER40802, No. DE-FG02-94ER40818, No. DE-FG02-94ER40865, No. DE-FG02-99ER41099, and No. DE-AC02-06CH11357, by U.S. NSF Grants No. 9603486, No. 0072204, and No. 0245011, by Polish MNiSW Grant No. NN202 282234 (2008–2010), by NSC of Taiwan Contract NSC 89-2112-M-008-024, and by Hungarian OTKA Grant (No. F 049823).

[1] I. G. Bearden *et al.*, Phys. Rev. Lett. **88**, 202301 (2002).
[2] B. B. Back *et al.*, Phys. Rev. Lett. **91**, 052303 (2003).
[3] B. B. Back *et al.*, Phys. Rev. C **74**, 021901 (2006).
[4] B. B. Back *et al.*, Phys. Rev. Lett. **93**, 082301 (2004).
[5] B. B. Back *et al.*, Phys. Rev. C **72**, 031901 (2005).
[6] B. B. Back *et al.*, Nucl. Instrum. Methods Phys. Res., Sect. A **499**, 603 (2003).
[7] M. Gyulassy *et al.*, Phys. Rev. D **44**, 3501 (1991).
[8] GEANT 3.211, CERN Program Library.
[9] B. B. Back *et al.*, Phys. Rev. Lett. **87**, 102303 (2001).
[10] Zi-wei Lin *et al.*, Nucl. Phys. **A698**, 375 (2002).
[11] http://www.phobos.bnl.gov/Publications/Physics/phobos_physics_publications.htm.
[12] B. B. Back *et al.*, Phys. Rev. C **74**, 021902(R) (2006).